Choosing the right electrode representation for modeling real bioelectronic interfaces: a comprehensive guide

Opančar, Aleksandar; Głowacki, Eric Daniel; Đerek, Vedran

Source / Izvornik: **Journal of Neural Engineering, 2024, 21**

Journal article, Published version
Rad u časopisu, Objavljena verzija rada (izdavačev PDF)

https://doi.org/10.1088/1741-2552/ad6a8b

Permanent link / Trajna poveznica: https://urn.nsk.hr/urn:nbn:hr:217:179432

Journal of Neural Engineering

PAPER

Choosing the right electrode representation for modeling real bioelectronic interfaces: a comprehensive guide

Aleksandar Opančar[1,2], Eric Daniel Głowacki[2,*] and Vedran Đerek[1,*]

[1] Department of Physics, Faculty of Science, University of Zagreb, Bijenička c. 32, 10000 Zagreb, Croatia
[2] Bioelectronics Materials and Devices Laboratory, Central European Institute of Technology, Brno University of Technology, Purkyňova 123, 61200 Brno, Czech Republic
[*] Authors to whom any correspondence should be addressed.

E-mail: glowacki@vutbr.cz and vdjerek@phy.hr

Keywords: bioelectronics, electrodes, interface, constant phase element, simulation

Supplementary material for this article is available online

OPEN ACCESS

RECEIVED
28 February 2024

REVISED
12 July 2024

ACCEPTED FOR PUBLICATION
1 August 2024

PUBLISHED
14 August 2024

Abstract

Objective. Producing realistic numerical models of neurostimulation electrodes in contact with the electrolyte and tissue, for use in time-domain finite element method simulations while maintaining a reasonable computational burden remains a challenge. We aim to provide a straightforward experimental-theoretical hybrid approach for common electrode materials (Ti, TiN, ITO, Au, Pt, IrOx) that are relevant to the research field of bioelectronics, along with all the information necessary to replicate our approach in arbitrary geometry for real-life experimental applications. *Approach.* We used electrochemical impedance spectroscopy (EIS) to extract the electrode parameters in the AC regime under different DC biases. The pulsed electrode response was obtained by fast amperometry (FA) to optimize and verify the previously obtained electrode parameters in a COMSOL Multiphysics model. For optimization of the electrode parameters a constant phase element (CPE) needed to be implemented in time-domain. *Main results.* We find that the parameters obtained by EIS can be used to accurately simulate pulsed response only close to the electrode open circuit potential, while at other potentials we give corrections to the obtained parameters, based on FA measurements. We also find that for many electrodes (Au, TiN, Pt, and IrOx), it is important to implement a distributed CPE rather than an ideal capacitor for estimating the electrode double-layer capacitance. We outline and provide examples for the novel time-domain implementation of the CPE for finite element method simulations in COMSOL Multiphysics. *Significance.* An overview of electrode parameters for some common electrode materials can be a valuable and useful tool in numerical bioelectronics models. A provided FEM implementation model can be readily adapted to arbitrary electrode geometries and used for various applications. Finally, the presented methodology for parametrization of electrode materials can be used for any materials of interest which were not covered by this work.

1. Introduction

The use of electronic devices in living systems for both electrical stimulation and recording requires a wide variety of bioelectronic methods and techniques, including single-cell patch-clamp for studying cell membrane properties, microelectrode arrays for cell culture or tissue stimulation and recording, all the way to the central nervous system and peripheral nerve implants for therapeutic and research purposes [1–7]. Stimulators can be external or implanted, wired or wireless, externally, or battery-powered [8–12], whereas stimulation protocols can be open- or closed-loop, continuous or intermittent, depending on the needs of the application. However, all modalities of electrical stimulation or electrical signal recording require a pair of electrodes as interfaces with the stimulation/recording target, where the current enters or leaves the region. The efficient and safe application of electric current to living cells or

tissues for purposes of either research or medical treatment is governed by the properties of the stimulation electrodes [13, 14]. Charge transport from the stimulation device to the electrode is electronic in nature, whereas in tissue, it is purely ionic [15]. The electrode/tissue interface is where the transduction of electronic to ionic transport occurs, and the physical properties of the electrodes, together with the stimulation protocol, determine if the electrical coupling will be capacitive, Faradaic, or of a mixed nature [16, 17]. A Faradaic electrode will facilitate the charge transfer by a redox reaction, either reducing or oxidizing chemical species in the surrounding environment or the electrode itself, resulting in the release of ions and free radicals, or in corrosion of the electrode. Typically, biphasic current pulsing protocols are applied to maintain charge balance, however, Faradaic charge transfer reactions may not be reversible and can cause net changes in the chemical environment surrounding the electrode [18]. Both processes can result in failure in stimulation and/or recording, as well as unwanted interactions of the living system with species released by redox reactions. Therefore, when designing stimulation devices and stimulation protocols, due attention should be paid to the electrodes, their geometry, and their electrochemical properties. Ultimately, only experiments will conclusively determine the safety and efficacy of the stimulation device, protocol, and electrodes [19, 20]. *In vitro* and *in vivo* experiments carry a substantial cost of time and resources, as well as an ethical burden, especially when iterations in design need to be statistically verified in large populations of laboratory model [21]. With rapid progress in computational capabilities, the concept of digital twins has been widely exploited to allow purely numerical experiments—simulations of a biological system in a reciprocal interaction with the environment—to supplement and reduce the necessity for real experiments, thus speeding up the research and reducing its financial and ethical burden [22–24]. A comprehensive digital twin simulation should include both the living and electronic sides of the system with a faithfully represented cell or tissue model, as well as the full model of the stimulation device. To fully comply with the requirements, all the digital twin model parameters should be dynamically updated by the real measurements. Finally, all components of the simulation must be individually experimentally verified, and the applicable range of the parameters established.

To fully describe electrical stimulation in bioelectronic systems, it is necessary to model the current injection from a bioelectronic device through the electrode, and into the electrolyte, where the current faces three-dimensional objects which may or may not be electrically active as well. Finally, the current is extracted through the return electrode. Provided that a faithful device model exists, it will be directly coupled to the stimulation and return electrodes, via the model of the environment. Several physical and electrochemical processes may occur at the electrode/electrolyte interface, such as formation of capacitive double layers or Faradaic reduction or oxidation processes, which may be further enhanced or limited by the transport of redox active species in the vicinity of the electrode in the electrolyte. Ab initio models considering all the species in the electrolyte, as well as the electrode material properties at the atomistic scale are neither feasible or reasonable with the current computational abilities, at least not for large spatial- and temporal-scale models. To efficiently numerically simulate the electrode response to a voltage stimulus in an electrolyte solution, a model with a minimal number of parameters is desired, considering its geometry, material, and electrochemical properties, especially in spatially extensive three-dimensional models where each spatial mesh element has multiple degrees of freedom associated with it. This electrode can then be coupled with other subsystems within a comprehensive numerical simulation.

We will show how said electrode properties can be extracted from simple electrochemical measurements, such as electrochemical impedance spectroscopy (EIS) with applied bias and fast amperometry (FA) under constant potential. Using the parameters extracted and estimated from those measurements, the electrode/electrolyte can be faithfully implemented in a three-dimensional time-dependent finite element method multiphysics model, which can be used for arbitrarily shaped electrical stimulation or recording. In particular, it is vital that the model is time domain based opposed to frequency domain to make it in principle compatible to a Hodgkin–Huxley type model which can be used to calculate the neural response. We will compare commonly used parametrizations of the electrode interface materials which are relevant to the field of bioelectronics research (gold, platinum, titanium, indium tin oxide, titanium nitride, and iridium oxide). The electrochemical properties of the material will be modelled as an equivalent Voigt RC circuit with voltage-dependent double layer capacitance and Faradaic resistance, and as the Randles circuit with voltage-dependent charge transfer resistance and constant phase element (CPE) parameters distributed along the electrode surface. We will demonstrate the implementation of both Voigt and Randles distributed equivalent circuits in the time-domain within the COMSOL Multiphysics environment. The parameters for both equivalent circuits will be extracted from the EIS measurements, and we will show that our model faithfully reproduces the measured EIS data in the frequency domain. We will show that the parameters extracted from EIS cannot be directly applied to pulsed stimulation, due to the inability of the EIS measurements to capture transient phenomena that can be present in low duty cycle

pulsed stimulation, due to transient changes in electrode properties or rapid depletion of redox-reactive species in the vicinity of the electrode when rapidly brought out of the equilibrium, especially when measuring the EIS under bias voltage. We will demonstrate and verify a method for self-consistent correction of the EIS parameters by nonlinear fitting of the equivalent circuit parameters to the fast amperometry measurements (FA), starting from the parameters obtained by the EIS. Finally, we will present the validation of our model by extrapolation to different geometries, changed electrolyte conductivity and stimulation protocols.

A number of recent works have tackled the numerical modelling of electrodes in contact with excitable tissues, each of which focused on a unique aspect of the problem, such as the electrode shape optimization [25, 26] or the studies of the effective electrical parameters at the stimulation target [27], while some have attempted to take into account also the electrochemical properties of the electrode [24] in the regime where no Faradaic reactions occur. Our attempt, however, includes a comprehensive FEM approach to the electrode impedance, using both distributed linear equivalent circuits and distributed CPE equivalent circuits, with all the parameters being extracted from the measurements and the model further optimized to reproduce the validation stimulation pulses. This approach has enabled us to identify both the materials and the electrical potential windows for which a simplified linear simulation approach may be valid. Furthermore, due to the used process of model validation by using the stimulation pulses, our model has inherent ability to be used as a digital twin, by feeding the measured data dynamically back to the model for validation and parameter optimization [22, 23].

To our knowledge, this is the first report of a non-approximate implementation of distributed electrochemical equivalent circuits with constant-phase elements in the time domain within the COMSOL Multiphysics FEM environment, as well as a unique comprehensive overview of electrochemical properties for commonly used electrode materials. Ultimately, the electrode model presented can be used to accurately represent an electrode/electrolyte interface used for stimulation or measurement in time domain, within a comprehensive finite element method simulation.

2. Method

2.1. Representation of electrochemical properties of the electrodes by equivalent circuit models

Electrodes in numerical simulations involving electrochemistry are typically represented by an equivalent electrical circuit. A concept of estimating electrical equivalent circuit parameters on an electrode to characterize its transport properties is advantageous, because the low number of parameters required for the model can be efficiently and rapidly solved using the state-of-the-art hardware, even with a massive number of degrees of freedom used in a simulation. There are many commonly used equivalent circuits, but two of the simplest and most commonly used are the Voigt circuit and the simplified Randles circuit with a CPE (figure 2) [28, 29].

The Voigt circuit (figure 2(a)) has the advantage of having a very clear interpretation of each element, containing an electrolyte resistance in series, with the double layer capacitance and charge transfer resistance in parallel. In addition, its numerical implementation is straightforward both in the time and frequency domains, since all elements can be represented by linear differential equations. On the other hand, the Randles circuit contains a CPE [30].

All equivalent circuit elements are well defined in the frequency domain by their complex impedances, $Z_R = R, Z_C = \frac{1}{j\omega C}$ and $Z_{\mathrm{CPE}} = \frac{1}{Q(j\omega)^{\alpha}}$, with α ranging from 0–1 for the capacitive CPE [31, 32]. The resulting impedance can be easily evaluated in the frequency domain, but can pose difficulties when implementing time-domain models.

It can be seen from the complex impedances that CPE falls somewhere in between the resistor and the capacitor depending on the exponent α, where $\alpha = 0$ reproduces the resistor and $\alpha = 1$ the capacitor with the parameter Q having the role of conductance and capacitance respectively. CPE with exponent α between those limiting values has a rather complex physical interpretation, but it models a behaviour very commonly encountered in electrochemistry.

The CPE behaviour of the electrode can either be an intrinsic microscopic property of the material, or a global behaviour originating from distribution of reactivity due to interface inhomogeneities such as surface disorder and roughness, electrode porosity, specific ion adsorption, electrode geometry and normal-to-surface distributions of properties in films and coatings [33]. In all the mentioned cases, it results from a 2D variation of properties along the surface of the electrode or 3D variation of properties also in the direction normal to the electrode surface [34]. Putting aside the microscopic properties of the electrode which can lead to a CPE behaviour, even an ideally capacitive electrode will have an apparent CPE behaviour above a certain limiting frequency f_{lim} due to the finite size of the electrode and the edge effects, leading to inhomogeneous electric field distribution across the electrode surface [35, 36]. Here, the apparent CPE behaviour refers to the fact that CPE exponent α is a function of frequency which is not the case for a normal CPE element. For the disc electrode of radius r the expression for f_{lim} is given by $f_{\mathrm{lim}} = \frac{\kappa}{2\pi C r}$, where κ is the electrolyte conductivity and C is the specific capacitance of the electrode [33].

For an electrode with a radius of 1 mm, the capacitance C can span a range of two orders of magnitude for commonly used materials, from approximately 10 μF cm^{-2} for indium tin oxide (ITO) to 1000 μF cm^{-2} for iridium (IV) oxide (IrOx). That gives the range of f_{lim} from 2.4 kHz to 24 Hz, well within the typical frequency range used in bioelectronics, which makes the effects of f_{lim} crucial for consideration of these applications.

In our work, we will use both Voigt and Randles equivalent circuits to represent electrochemistry on the electrode surface, to evaluate the optimal conditions in which they may be used. Further, we will consider all of the equivalent circuit parameters to be in principle voltage-dependent.

2.2. Electrode preparation

Microscope slides (1 × 1) inch^2 were cleaned by successive ultrasonication in acetone, isopropanol, Micro-90 detergent, and DI water, and finally treated with oxygen plasma (Diener NANO Plasma Cleaner). All samples were then sputter coated with a 100 nm layer of Ti using a Kaufman ion-beam source (IBS). This Ti acts as a common layer below all studied samples with the exception of ITO, as it has excellent adhesion on glass and is a suitable underlayer for all the studied materials. Platinum or Gold (60 nm) is deposited using DC magnetron sputtering. TiN (60 nm) is reactively sputtered from a Ti target using two IBS, the latter generating a nitrogen ion beam, according to [37]. IrO_x was obtained via DC reactive magnetron sputtering in an Ar/O_2 plasma (100 nm) according to previous published methods [38]. ITO on glass was used as purchased, from Kintec, 10 Ohm/square. In short, all materials consisted of a thin film deposited by a PVD method of choice on 25.4 × 25.4 mm^2 cleaned glass substrates. Active electrochemical electrode area was defined by masking the substrates with adhesive polyimide stencils. The electrode area on the stencil was defined by laser cutting a circle with the diameter of 2 mm. Additionally, for validation of extrapolation experiments stencils with diameters of 0.5, 1, 2, 4 and 6 mm were applied on prepared electrodes.

2.3. Electrochemical measurement setup

Electrodes were placed in one side of a double-tank electrochemical cell (MM double-tank cell, *Redox.me*). The working electrode (WE) with an active area of 3.25 mm^2 was fixed on one side, while the counter electrode (CE) was placed on the other side, separated by 20 mm. The electrolyte used for the measurements (1× PBS) was prepared from Roti-CELL 10x Dulbecco's Phosphate-Buffered Saline without Ca and Mg by diluting it in 1:9 ratio with DI water according to the manufacturer specifications, giving a 140 mM concentration of Cl^- in the final solution. A 10× diluted version of the same electrolyte, 0.1x PBS, was prepared by diluting the 1xPBS in 1:9 ratio with DI water. An Ag/AgCl wire was used as a reference electrode (REF) and placed 5 mm from the WE. The electrodes were connected to the corresponding ports by alligator clips to a PalmSens 4 or Ivium PocketStat2 potentiostat, or alternatively to a combination of a potentiostat and a digital oscilloscope (Pico Technology, Picoscope 4424 A).

2.4. EIS

EIS was measured in a 3-electrode setup, using the phosphate-buffered saline (PBS) as an aqueous electrolyte and a platinum CE. Measurements were conducted with PalmSense4 potentiostat at a DC voltage bias V_P, ranging from −900 + 800 mV in steps of 100 mV vs. Ag/AgCl reference wire, in a frequency range of 100 mHz–100 kHz with 8.5 frequencies per decade (52 frequencies in total per DC bias.) The AC amplitude was set to 10 mV for all measurements.

2.5. FA

FA was measured in the same electrochemical cell and under the same conditions as the EIS measurements. Current response to the constant voltage pulses applied to the WE, ranging from −900 + 800 mV in steps of 100 mV vs. Ag/AgCl was measured We allowed 1 min between the application of successive voltage pulses to allow the electrode to equilibrate, which we verified by applying the voltage pulse of the same voltage and making sure that the current transients perfectly overlap. Typical electric stimulation protocols involve voltage or current pulses; therefore, the resulting current decay traces are representative for the common stimulation scenarios and were used later for model adjustment and validation.

FA measurements were performed using a PalmSens4 potentiostat and a digital oscilloscope or an Ivium PocketStat2 potentiostat. Both models of used potentiostats exhibit an operational feature manifested as a short delay in transient current measurement immediately after a voltage pulse. For PalmSense4 that delay is approximately 110 μs and for PocketStat2 it is around 165 μs. Therefore, when using PalmSens4 the current transients were measured by a digital oscilloscope, measuring a voltage drop on a 100 Ohm resistor placed in series with the potentiostat and the electrochemical cell, while with the PocketStat2 with a longer pre-trigger period the delay could be avoided.

2.6. Cyclic voltammetry (CV)

CV scans were performed before the EIS measurements to estimate the capacitive window for each material and after the EIS measurements to ensure that there were no significant changes in electrode performance. In addition to that, in the case of iridium oxide, repeated CV scans were performed

to electrochemically activate the electrode until we could see a stable cyclic voltammogram. CV scans were performed with Palmsense4 potentiostat from −0.9–0.8 V vs Ag/AgCl reference wire with a scan rate of 1 V s^{-1}.

2.7. Steady-state parameter extraction

Measurement of the electrochemical impedance spectra enables the estimation of the equivalent circuit parameters for different electrodes, by numerical fitting of the measurements to a selected equivalent circuit model. Over time, the EIS instrumentation has evolved to the state where portable EIS-enabled potentiostats became a common laboratory commodity, with the included software greatly simplifying the experiments and data evaluation. Thus, our focus is on using simple EIS measurements to model and obtain equivalent circuit parameters for selected electrodes using the appropriate equivalent circuit. To find an equivalent circuit that would accurately predict the electrode behaviour for a wide range of voltages and frequencies, voltage-biased EIS measurements were performed on all the samples.

In the simplest approximation, the entire electrode surface is modelled as one equivalent circuit. However, realistic electrodes may not have an equipotential surface or may not be spatially homogeneous—thus, it is advantageous to represent the electrode as a distribution of equivalent circuits. The former approach will be used in modelling the EIS data, while we will use the latter approach in our FEM numerical model.

Firstly, we modelled the measured data for each voltage bias V_P to a simple RC Voigt circuit (figure 2(a)). A linear RC Voigt circuit is simple to implement in numerical simulations, and thus is widely used. However, it does not consider the reaction kinetics, which cannot be modelled by a simple RC circuit, and may introduce significant errors in a numerical simulation. However, it may be appropriate to model some of the electrode materials in a limited range of applied voltage. Secondly, we modelled the measured data to a Randles circuit with a CPE (figure 2 (b)). The Randles circuit with the CPE considers the reaction kinetics and diffusion behaviour and has provided a much better fit for all materials. From the best numerical fit, we obtained the values of $R_{CT}(V_P)$, $Q(V_P)$ and $\alpha(V_P)$, as well as of the electrolyte resistance R_s. From the obtained voltage dependent equivalent circuit parameters $R_{CT}(V_P)$, $Q(V_P)$ and $\alpha(V_P)$ we calculate the distributed electrode parameters (figures 1(b) and (c)). To obtain the Voigt RC parameter from the single Randles equivalent circuit, we follow the approach outlined by Brug *et al* [30, 39] and use the formula:

$$C_{DL} = Q^{\frac{1}{\alpha}} \left(\frac{R_S R_{CT}}{R_S + R_{CT}} \right)^{(1-\alpha)/\alpha},$$

where the parameters Q, R_S, R_{CT} and α are obtained by fitting the measured EIS data to the Randles circuit (figure 2(b)).

If we assume that the electrode surface is homogeneous i.e. that the local surface properties are identical for the entire electrode area, then each microscopic surface element has the same local equivalent circuit describing it as in figure 1(c). Since all of the local equivalent circuits are connected in parallel, the admittance of the entire electrode corresponds to the integral of the local circuits' admittance across the entire electrode area.

$$Y_{total} = \int Y_s dA = Y_s \int dA = Y_s A,$$

where the second equality is due to the homogeneity of the electrode.

Thus, we can calculate the local electrode properties for both microscopic electrode descriptions, Randles CPE ($Q_{SPEC}, \sigma_{CT}, \alpha$) and Voigt RC ($C_{SPEC}, \sigma_{CT}$) by dividing the total electrode admittance by the area of the electrode, obtaining the local electrode parameters:

$$Q_{SPEC} = \frac{Q}{A}, C_{SPEC} = \frac{C_{DL}}{A}, \sigma_{CT} = \frac{{R_{CT}}^{-1}}{A}.$$

It is important to note that the series electrolyte resistance R_S emerges from the geometry of the FEM simulation and the electrolyte conductivity κ and is not implemented as an electrode property. For actual simulations, we add an additional 50Ω series resistance to compensate for the contact resistance of the electrode and 100Ω series resistance that represents shunt resistor used in the FA measuring setup. We choose the added resistance to replicate high-frequency series resistance measured by EIS.

2.8. COMSOL model implementation

The WE, CE and REF, as well as the surrounding electrolyte were implemented in COMSOL Multiphysics 6.0, using the Electric Currents interface of the AC/DC module. We exploited the symmetry of the problem, solving it in 2D axisymmetric geometry, which greatly reduces the complexity of the calculated problem in comparison to the full 3D model. WE and CE were implemented as the 2D boundaries with an appropriate boundary condition distributed along the electrode surface, while the electrolyte was modelled as a 3D isotropic conductive medium characterized by the relative permittivity $\epsilon_r = 77$ and conductivity $\kappa = 1.5\ S\,m^{-1}$ or $0.15\ S\,m^{-1}$ in the case of 1x PBS and 0.1x PBS respectively. The REF electrode is defined as an equipotential region where the electric V_{REF} potential is probed, connected to a very high impedance potentiostat input. The complete geometry with the boundary conditions is shown

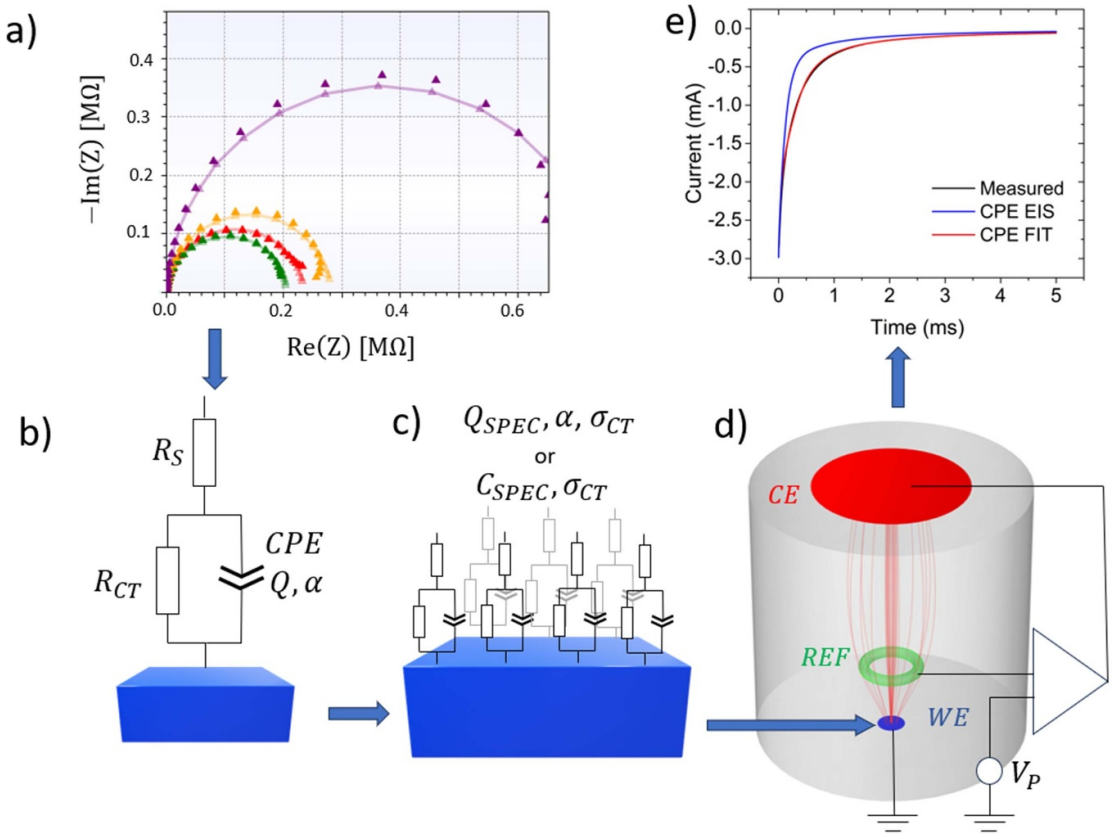

Figure 1. A schematic workflow of methodology for modelling an arbitrary electrode and evaluating the model. Firstly, the electrode is characterized by electrochemical impedance spectroscopy (EIS), with different constant potential (DC) biases extending beyond the limits of the electrochemical window for a given material. In addition, current response to constant voltage pulses for each of the materials is measured by fast amperometry (FA). EIS parameters are fitted to a chosen equivalent circuit electrode representation, with the results implemented as a distributed electrode interface in the 3D FEM software (COMSOL Multiphysics), in the time domain. The current response to a voltage pulse is evaluated from the FEM model, and compared to the FA measurements. The EIS parameters of the model are iteratively optimized to obtain the best fit of a model to the FA measurements. (a) EIS measurements for different DC biases, with Z representing the measured complex impedance (b) fitting of the measured EIS data to the appropriate equivalent circuit, with R_{CT} representing the charge transfer resistance, R_S the electrolyte series resistance, CPE a constant phase element with the CPE parameter Q and the CPE exponent α; (c) calculating the distributed (intensive) electrode parameters for the Randles equivalent circuit electrode representation (CPE parameter Q_{SPEC} and the CPE exponent α), or Voigt equivalent circuit C_{SPEC}, and the charge transfer conductance σ_{CT} from the single equivalent circuit (extensive) parameters, (d) implementing the distributed parameters in the 3D FEM time-dependent COMSOL model with the control voltage V_P delivered by a potentiostat between the working electrode (WE) and the reference electrode REF, by adjusting the bias between the WE and the counter electrode CE; (e) simulating the current response (CPE FIT and CPE EIS) to the short voltage pulse and comparing to the measurements obtained by Fast amperometry.

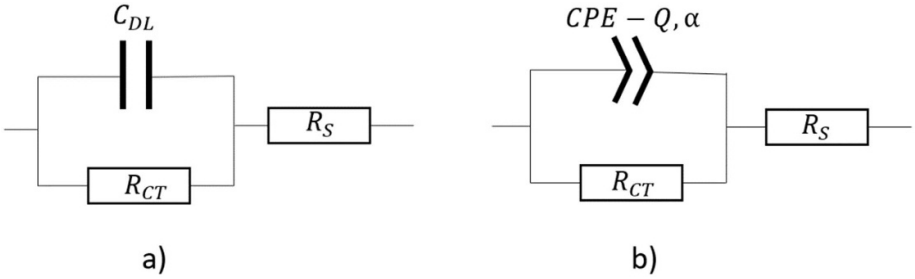

Figure 2. Schematic representations of (a) Voigt and (b) simplified Randles equivalent circuits, with C_{DL} representing electrochemical double-layer capacitance, R_{CT} charge transfer resistance, R_S electrolyte series resistance, CPE a constant phase element with CPE parameter Q and the CPE exponent α.

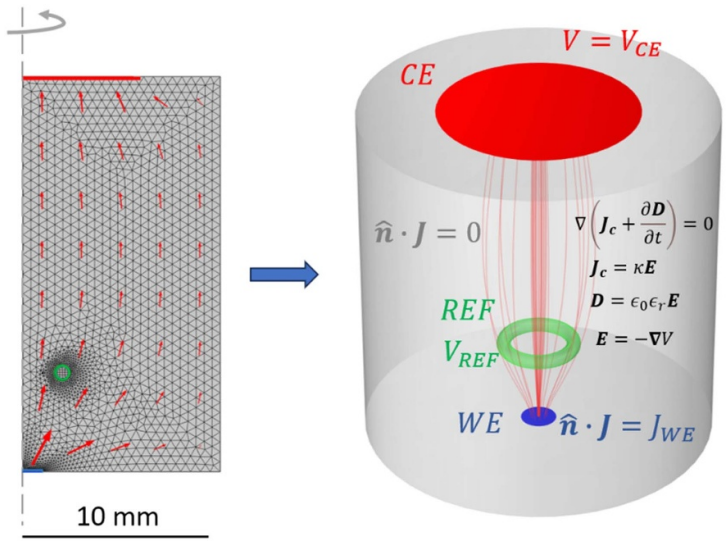

Figure 3. 2D and the corresponding 3D rotated axisymmetric geometry with mesh depicted in the 2D image and denoted boundary conditions and governing equations in the 3D. Current density is visualized by red arrows and lines.

in figure 3, showing the 2D and the corresponding 3D rotated axisymmetric geometry. The volume was meshed in COMSOL Multiphysics using the Delaunay Triangular mesh with element size ranging from 0.05 mm on the WE to 0.5 mm on the CE.

The Robin boundary condition on the WE is defined by the local normal current density on the WE J_{WE} [40]:

$$\hat{\boldsymbol{n}}\cdot\boldsymbol{J} = J_{WE}.$$

The expression for J_{WE} is calculated for every surface mesh element of the WE and has two contributions, capacitive charge density accumulating on the electrode surface σ_{WE} and the Faradaic current density transferred across the electrode interface J_F:

$$J_{WE} = \frac{\mathrm{d}\sigma_{WE}}{\mathrm{d}t} + J_F.$$

J_F and σ_{WE} are calculated according to the specifics of the equivalent electrical circuit used. For the Voigt RC circuit, σ_{WE} is the surface charge density σ_C of the ideal capacitor given by:

$$\sigma_{WE} = \sigma_C = C_{SPEC} V_{WE},$$

where V_{WE} is the voltage on the electrode-electrolyte interface along the WE and C_{SPEC} is the specific capacitance of the electrode which may be a function of V_{WE}.

We calculate V_{WE} as the difference of the electric potentials across the electrode-electrolyte interface $V_{WE} \equiv V_M - V_{el}$, where V_{el} is the electric potential of the electrolyte mesh elements adjacent to the WE and V_M is the potential of the metal electrode, which is in our case grounded via the potentiostat circuit. V_{el} is spatially dependent and calculated for each mesh element adjacent to the electrode surface whereas V_M is approximated as equipotential for the entire electrode. This is justified because the conductivity of the electrode metal is much greater than the conductivity of the electrolyte so the difference in electric potential on the electrode side can be neglected compared to the potential variation along the electrode on the electrolyte side of the interface.

In case of the Randles circuit, σ_{WE} corresponds to the surface charge density of the CPE σ_{CPE} which is given by the expression:

$$\sigma_{WE} = \sigma_{CPE} = \int_0^t \frac{Q_{SPEC}}{\Gamma(1-\alpha)} \frac{V_{WE}}{(t-\tau)^{\alpha}}\,\mathrm{d}\tau$$
$$t > 0; 0 < \alpha < 1\,, \qquad (1)$$

where Q_{SPEC} and α are CPE parameter and exponent, Γ is the gamma function and t is the time from the beginning of the simulation [41]. Q_{SPEC} and α may be functions of V_{WE}. What makes this implementation much more complicated and computationally demanding than the Voigt circuit implementation is the explicit dependence of the integrand on time in the above expression. The explicit time dependence forces us to solve the above integral anew for every mesh element in the electrode for each time step of the solver, which makes the computation much slower and gives rise to additional constraints on the time stepping while solving as well as some difficulties specific to COMSOL outlined in section 2.9 and the supporting information sections 1 and 2. A possible simplification to significantly speed up the computation would be considering only a single CPE element that represents the entire electrode instead of the distributed CPE mesh. That would require solving the integral in equation (1) only once per time step

instead of solving it for every electrode mesh element. On the other hand, that kind of simplification would not allow us to get the accurate electrode response at frequencies higher than f_{lim} or equivalently times shorter than $1/f_{\mathrm{lim}}$ as demonstrated in section 5.1 [35, 42].

In both cases, the Faradaic current density is given by the Ohms law:

$$J_{\mathrm{F}} = \sigma_{\mathrm{CT}} V_{\mathrm{WE}},$$

where σ_{CT} is the charge transfer conductivity, a function of WE voltage V_{WE}.

Since the reference electrode is connected to a very high impedance input of a potentiostat we require that there is no net current flowing through the reference electrode surface ∂REF:

$$\oint_{\partial \mathrm{REF}} \hat{\boldsymbol{n}} \cdot \boldsymbol{J} \mathrm{d}A = 0.$$

On the counter electrode such potential V_{CE} is applied that the voltage between WE and REF is precisely the control voltage set by the potentiostat V_{P}. The rest of the boundaries have the Electric insulation boundary condition given by:

$$\hat{\boldsymbol{n}} \cdot \boldsymbol{J} = 0.$$

The equation for the electric potential in the electrolyte bulk is derived by taking the gradient of the Ampere's law and considering the identity $\nabla \cdot \nabla \times \boldsymbol{B} \equiv 0$:

$$\nabla \left(\boldsymbol{J_c} + \frac{\partial \boldsymbol{D}}{\partial t} \right) = 0.$$

After relating the conduction current density in the electrolyte $\boldsymbol{J_c}$ to electrical field with Ohm's law with bulk conductivity κ:

$$\boldsymbol{J_c} = \kappa \boldsymbol{E}$$

and taking the constitutive relation for $\boldsymbol{D}$:

$$\boldsymbol{D} = \epsilon_0 \epsilon_r \boldsymbol{E},$$

finally, the electric field is connected to the electric potential by a negative gradient:

$$\boldsymbol{E} = -\nabla V.$$

2.9. Time-domain implementation of the CPE

The additional difficulty with the CPE implementation arises from the fact that coupling of the computed potentials at former time steps back into calculation at current time step via integration is not possible in COMSOL 6.0. to the best of our knowledge. That makes the implementation of integral in equation (1) impossible with available methods for time integration within COMSOL. To circumvent that issue, we needed to make the entire history of the computed potential available at each time step for every mesh element of the electrode. We achieve this by mapping the entire computed history $V_{\mathrm{WE}}(r,t)$ into a spatial variable $U(r,z,t)$ that we can then integrate over with spatial integration methods. For this mapping purpose we added the stabilized convection–diffusion equation interface of the COMSOL Mathematics module and constructed a dedicated geometry for potential mapping, depicted in the supporting information figure S1.

We define the 1D convection equation for the mapping variable U:

$$\frac{\partial U(r,z,t)}{\partial t} + \beta \frac{\partial U(r,z,t)}{\partial z} = 0$$

and we set the value of convection coefficient β to -1 m s^{-1}. This means that we will have 1:1 temporal to spatial mapping where $U(r,z,t) = U(r,z+\beta\tau, t+\tau)$.

We connect the variable U to the potential V_{WE} with boundary and initial conditions. We define a Dirichlet boundary condition:

$$U(r,0,t) = V_{\mathrm{WE}}(r,t)$$

and the initial condition:

$$U(r,z,0) = V_{\mathrm{WE}}(r,0) = 0$$

because we start the simulations with zero voltage on the electrode.

The connection of U to V_{WE} is then given by:

$$W_{\mathrm{WE}}(r,\tau) = U(r,0,\tau) = U(r, z=\beta(t-\tau), t).$$

Finally, by substitution we can rephrase the integral in equation (1) in terms of spatial integration of variable U:

$$\sigma_{\mathrm{CPE}}(r,t) = \int_0^{\beta t} \frac{Q_{\mathrm{SPEC}}}{\Gamma(1-\alpha)} \frac{U(r,z,t)}{\beta(t-z/\beta)^{\alpha}} \mathrm{d}z \quad t>0; 0<\alpha<1.$$

We evaluate this integral using the *linproj* operator in COMSOL 6.0. Additional details of the implementation can be found in the supporting information sections 1 and 2. The COMSOL model file, pdf report and supporting data can be obtained from the repository[43] referenced in the data availability statement.

2.10. Transient parameter optimization

In addition to EIS, we have also measured the current response to constant voltage pulses applied to the electrodes by FA and by using those measurements we evaluate our final electrode model. We cannot expect that the equivalent circuit with parameters obtained from EIS will work perfectly for the fast voltage pulse transients in the time domain, as the biased EIS measurement protocol establishes the DC equilibrium state before starting AC measurement, and thus it may miss some of the dynamic processes

that play a key role in the case of fast pulses, such as the dynamics of the oxygen reduction and other Faradaic reactions at the electrodes. The reason for that is that EIS measurements can, for example, quickly deplete oxygen locally available at the electrode even before the impedance measurement begins, and as a result the process becomes diffusion limited, which is not the case to the same extent for the voltage pulses at the millisecond time scale [18]. We can, however, find the equivalent circuit which will accurately represent the electrode in the stationary EIS limit and hopefully, by small adjustments, we can have a good fit on the current transients measured by the FA. Thus, to improve the model's results, we did a series of numerical optimizations of the equivalent circuit parameters starting from the EIS data, by using *BOBYQA* algorithm in the Parameter Estimation study of the Optimization module of COMSOL 6.0. We varied the values of Q_{SPEC} and C_{SPEC} to obtain the best least-squares fit to the measured data.

This adjustment is not trivial because the circuit parameters $Q_{\mathrm{SPEC}}(V_{\mathrm{WE}})$ and $C_{\mathrm{SPEC}}(V_{\mathrm{WE}})$ are functions of electrode voltage and for each pulse the voltage on the electrode changes from $V_{\mathrm{WE}}(t=0) = 0$ to $V_{\mathrm{WE}}(t=t_{\mathrm{P}}) \approx V_{\mathrm{P}}$ where t_{P} and V_{P} refer to the pulse duration and pulse voltage respectively. That means that for each voltage pulse we need to fit a function rather than a simple number for Q_{SPEC} and C_{SPEC} which drastically complicates the fitting procedure and does not guarantee a unique result for each pulse due to possible local minimums that the fitting procedure may encounter. To solve this issue, we use the following fitting procedure.

First, we fit to the voltage pulses of the smallest amplitude $V_P = V_{P\pm1} = \pm 100$ mV vs Ag/AgCl electrode for anodic and cathodic pulse. We can fit the values for Q_{SPEC} and C_{SPEC} for the limiting $V_{\mathrm{WE}} = V_{P\pm1}$ only and assume that for the voltages $V_{P-1} < V_{\mathrm{WE}} < V_{P+1}$ the parameters Q_{SPEC} and C_{SPEC} change linearly between the end values. That assumption is well justified if the electrode parameters do not change drastically within the voltage resolution of our measurements $\Delta V = |V_{P+1} - V_{P-1}|$.

Next, we fit on the pulses of the second smallest amplitude$V_{\mathrm{P}} = V_{\mathrm{P}\pm2} = \pm 200$ mV vs Ag/AgCl. We again fit the values for Q_{SPEC} and C_{SPEC} for the limiting values $V_{\mathrm{WE}} = V_{P\pm2}$ only and assume that the parameters change piecewise linearly between $V_{P-2} < V_{\mathrm{WE}} < V_{P-1}$ and $V_{P+1} < V_{\mathrm{WE}} < V_{P+2}$ where the values for the parameter between V_{P-1} and V_{P+1} are fixed from the previous two pulses and are not subject to further change.

We thus repeat the same procedure for all the voltage pulses in the ascending order of voltage amplitude. In this way we only fit a single value for Q_{SPEC} and C_{SPEC} for each pulse and reduce the fitting procedure to a series of single variable fits, making the entire procedure computationally simple and numerically robust. Voltage dependent electrode parameters $Q_{\mathrm{SPEC}}(V_{\mathrm{WE}})$, $C_{\mathrm{SPEC}}(V_{\mathrm{WE}})$ and $\sigma_{\mathrm{CT}}(V_{\mathrm{WE}})$ are implemented in COMSOL by using the built-in interpolation function feature which creates an analytic function from the parameter values measured or fitted with some finite voltage resolution. These interpolation functions are used in the physics governing equations as the parameter values. In this way the parameter values are dynamically updated at every solver time step to have the value prescribed by the functional dependence given the value of V_{WE} at that exact time step.

3. Results and discussion

We have built our 3D FEM model to faithfully represent the geometry of the measured electrochemical cell. The fundamental microscopic (material-dependent) electrode parameters were parametrized by two equivalent circuits, Voigt (RC) and Randles (CPE), applied to the electrode mesh elements. While the choice of the Voigt RC circuit may be naïve, it is very commonly used due to the ease of implementation, and we will show in which cases it may still be used. On the other hand, the Randles equivalent circuit can model the measured electrodes faithfully, while unfortunately introducing increased complexity to the model's implementation. There are a few key insights from these results that will guide us in the choice of the most appropriate equivalent circuit. First, in all of the EIS measurements, we see the presence of the CPE characterized by 'depressed semicircles' in the Nyquist plot or flat plateaus visible in the phase component of the Bode plot shown in the supporting information figures S2–S7. That implies that we must use an equivalent circuit with a CPE element, such as a Randles circuit, if we want to obtain an accurate fit. Secondly, the values of the fitted parameters for the same material vary greatly for different DC biases. That means that we must allow for voltage-dependent parameters in our equivalent circuit.

As mentioned in 2.1, the observed CPE behaviour can be the result of a 2D or 3D variation of electrode properties or, above the limiting frequency f_{lim}, the result of the inhomogeneous electric field distribution along the electrode surface. If the reason for the observed CPE behaviour is one of the former two, there is no other choice than to use the Randles circuit (figure 2(b)) both for fitting the EIS data (figure 1(b)) and as a distributed microscopic description of the electrode surface that we implement in the FEM simulation (figure 1(c)). If the latter is the reason for the observed CPE behaviour, the Randles circuit must still be used to fit the EIS measurements, but there is the possibility that the microscopic electrode parameters can be well described by a simpler Voigt RC circuit (figure 2(a)) and that we will obtain the

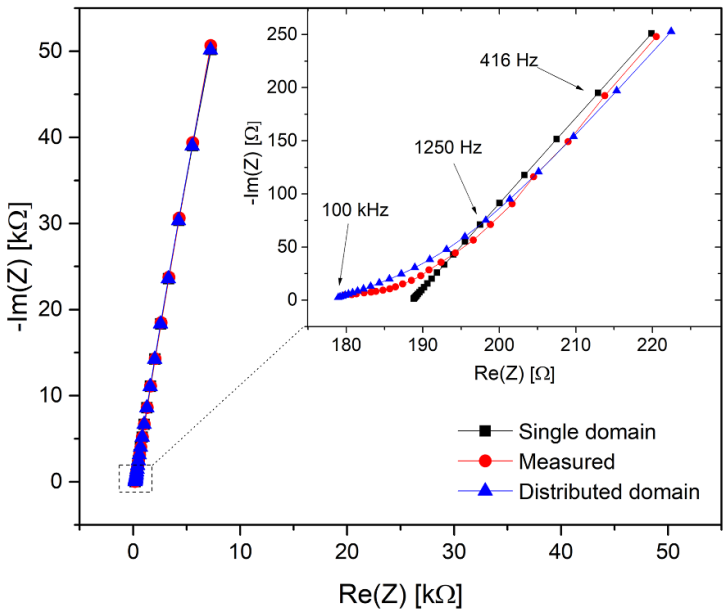

Figure 4. A Nyquist plot of the measured, fitted and FEM simulated EIS spectrum for a gold electrode, demonstrating the advantage of a distributed equivalent circuit in a FEM model in comparison to using a single domain EIS equivalent circuit in the high-frequency region.

observed CPE behavior 'for free' as a result of the realistic 3D FEM distributed electrode model instead of the single equivalent circuit.

We will not try to a priori determine if the microscopic RC description is completely justified or not; rather we will present both implementations and report on the relative error of using each microscopic description. The reader then has to determine whether the relative error associated with each description is acceptable for their specific application.

Once our model is verified by comparing it to the measurements, the electrode parameters can be applied to arbitrary electrode geometries, such as in multi-electrode arrays or other electrodes of choice. We will demonstrate the power of extrapolation of the model by applying it to different geometries, stimulation protocols and electrolyte environments.

3.1. Model verification by EIS

To verify our implementation of the 3D electrode model in the time domain, we firstly replicate the results obtained from EIS by doing the time domain simulations for the small AC perturbation and using the inverse Fourier transform to get the frequency dependent impedance data. We calculate the local equivalent circuit parameters (section 2.7) from fitting the EIS data to single Randles circuit (figure 2(b)) and implement them in our model in a distributed form (figure 1(c)). We compare the numerically modelled result with the impedance spectra fitted to a single Randles circuit and the measured data. Here we show only the representative results for a gold electrode (figure 4). A good match over the whole measured spectrum was found for Au, as well as for other materials, with the high frequency region for the Au electrode shown in the inset. We can see that all the data are in good agreement for lower frequencies, tracing almost a perfect straight line in the Nyquist plot characterized by the CPE coefficient $\alpha = 0.921$. Above the limiting frequency (426 Hz for the gold electrode) the measured and simulated distributed data deviates from the trend, with significant differences above three times the limiting frequency. The reason is that a 3D model can capture the variations in potential close to the electrode edge, whereas a single equivalent circuit cannot. In our FEM model every mesh element behaves as a separate equivalent circuit; thus, our model is shown to reproduce the physics more realistically than a simple single domain equivalent circuit obtained from the EIS [35, 42].

3.2. Model verification by FA

Electrical stimulation protocols commonly employ pulsed stimulation, which displays complicated temporal dynamics changing from kinetic to diffusion controlled regimes as the pulse progresses—in contrast to the EIS measurements, which show responses to single sinusoidal frequencies after the DC equilibrium is established. Thus, the model needs to be verified for the intended usage scenario. Voltage pulses within a range of amplitudes, typically within the electrochemical window of water-based electrolytes, were applied to all electrodes, and current transients were recorded.

Firstly, we used the voltage dependent parameters for the distributed Randles and Voigt equivalent

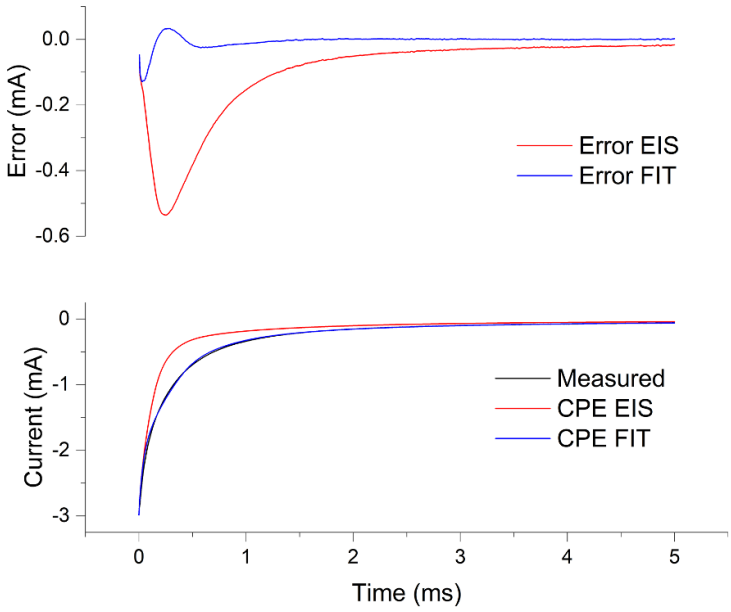

Figure 5. Simulated and measured current traces as a response to a 5 ms square −900 mV voltage pulse for the TiN electrode. The current trace modelled from the parameters obtained by EIS is underestimating the transferred charge. Deviations from the measured data are shown in the upper panel.

circuits obtained from EIS and plugged them directly into our model. As can be seen in figure 5, the resulting traces, even for the CPE fit, differed significantly from the measured data, most likely due to the dynamics of the electrode which was not captured fully by the EIS measurements. To improve the model's results, we did a series of numerical optimizations of the equivalent circuit parameters starting from the EIS data. The comparison of voltage-dependent Voigt circuit parameters (σ_{CT} and C_{SPEC}) and Randles circuit parameters (Q_{SPEC} and α) obtained from EIS, and optimized to the measured data, starting from the EIS parameters, are shown in figure 6.

We observe large differences between steady state parameter obtained by EIS and transient parameters obtained by fitting to FA measurements in all the measured materials at some potential regions. We hypothesize that in all cases the difference originates from Faradaic reactions which will not be apparent in EIS to the extent which they are visible in FA because in EIS method the system must assume a steady state at given DC bias before applying AC perturbation. This DC equilibrium will deplete reactants close to the electrode thus making a reaction seem much less prominent than in a short pulse transient where the reactants are present in the equilibrium amount near the electrode surface. In particular, gold electrode in the cathodic region showed almost five times greater CPE parameter in transient than predicted by EIS and we can attribute that difference specifically to the to the oxygen reduction reactions according to [18]. Finally, we present parametrizations for the Randles and Voigt circuits that provide the best fit on the FA pulses on each of the measured materials and report the errors for the two implementations.

EIS measurements can provide a good parametrization for different electrodes operated in pulsed mode near their open circuit potentials (OCP). For pulse voltages further from their OCPs the EIS parameters can serve as a good starting point for further optimization.

3.3. Voigt versus Randles implementation

As mentioned, the Voigt RC equivalent circuit is often implemented in time-domain simulations, due to the rather simple numerical implementation.

To quantify the agreement between measured and simulated data we introduce the error metric as a measure of relative difference between the simulated and measured delivered electric charge:

$$\text{Error} = \frac{\int |I_S - I_M| \, dt}{\int |I_M| \, dt}$$

where I_S and I_M are simulated and measured current. We calculated the error metric for each voltage pulse for every material (figure S9). The error metric averaged across voltages for different materials is shown in figure 7 with error bars indicating standard deviation of the error metric for the different voltages.

With the Randles circuit (CPE) it is possible to obtain good agreement between measured and simulated data with an average error below 10% for all the measured materials. With the Voigt circuit (RC), the average error is seen clearly increasing with decreasing CPE exponent α. Great care should be taken when

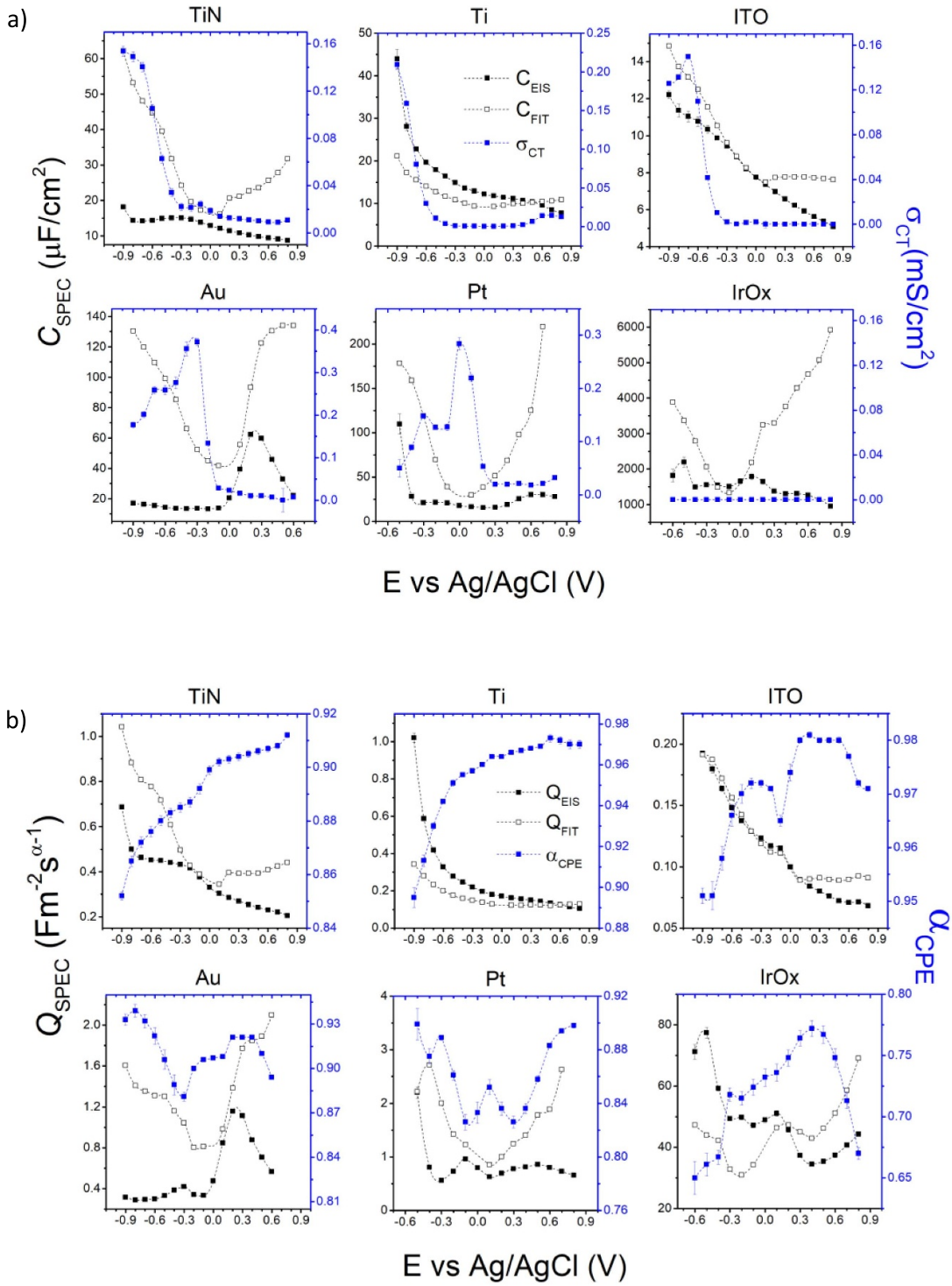

Figure 6. (a) Results of best fits of the voltage dependent (a) RC parameters—specific double layer capacitance $C_{SPEC}$and charge transfer conductivity σ_{CT}, and (b) CPE parameters Q_{SPEC} and α_{CPE}, for titanium nitride, titanium, indium tin oxide, gold, platinum and iridium oxide. Parameters obtained from EIS are labelled EIS, fitted parameters that offer improved agreement with the measured data are labelled FIT. Voltages were measured vs. Ag/AgCl electrode. Error bars indicate fit uncertainty.

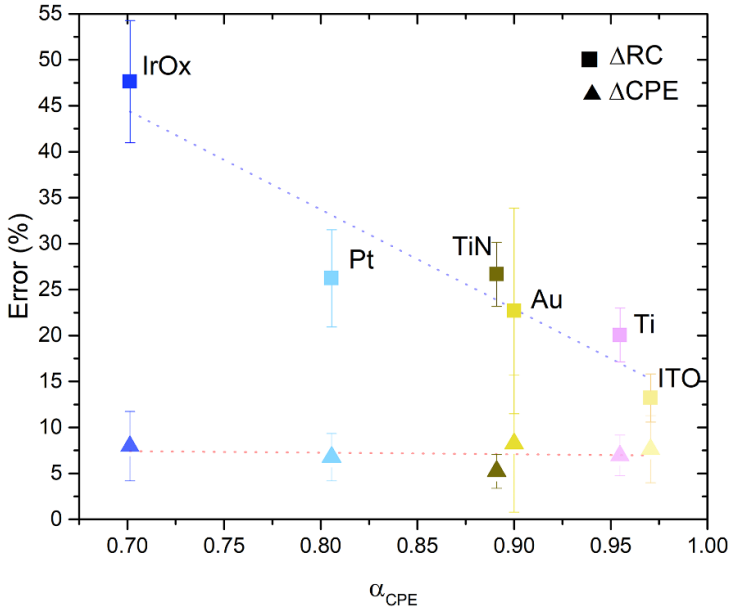

Figure 7. Average error (Δ) of modelled in comparison to the measured current traces for the RC and the CPE mode, for different materials. Error bars indicate standard deviation for all the voltage amplitudes for each material.

applying RC parametrization to materials with $\alpha \leqslant 0.9$ as the possible error is above 25%.

3.4. General model applicability

To determine the applicability of our model in more general cases as well as the limitations of the model we performed additional experiments varying electrode size, electrolyte concentration and stimulus shape and thus tested its extrapolation validity for certain cases. We chose to focus these experiments on a TiN electrode as a representative material due to the widespread use for electrical stimulation as well as its median position for CPE exponent (figure 7).

3.4.1. Variations in electrode size and electrolyte concentration

We performed FA measurements for the combinations of 5 different electrode sizes (with diameters 0.5, 1, 2, 4 and 6 mm) and two electrolyte concentrations (1x PBS and 0.1x PBS). The parameters are extracted and fitted as explained in Chapter 4 only for the 2 mm electrode in 1x PBS. These parameters are then applied to all the other size/electrolyte combinations, simulated in COMSOL, and compared with the FA measurements. Comparison between simulated and measured currents as a response to a short voltage pulse is shown in figure 8.

We do not observe a particular trend in the agreement between measured and simulated currents for the different electrode diameters for neither of the electrolyte concentrations as seen in figure 8(d)). We also do not see the combination on which the parameter extraction was performed as particularly standing out from the rest of the data so we can conclude that the model works well for the measured variation in electrode sizes that spans 12 times ratio in diameter or 144 times ratio in surface area between the largest and the smallest measured electrode size.

We do observe a significant difference between the agreement for different electrolyte concentrations with 1xPBS, in which the parameter extraction was performed, outperforming 0.1x PBS in average error by about a factor of two. Even though that difference is significant, it can be put into perspective of the relative errors of different electrode model implementations (Voigt RC vs. CPE) where the RC model still performs significantly worse (figure 7) than the CPE model for a 0.1x PBS electrolyte concentration.

It is apparent in figures 8(b) and (c) that for 0.1x PBS the model systematically overestimates the current indicating the overestimation of the double layer capacitance. The same is also be predicted from theory of the Gouy–Chapman–Stern model of the double layer capacitance where the capacitance increases with electrolyte concentration but levels off at high electrolyte concentrations [44]. Since we are doing 10x dilution of the electrolyte we might be seeing this reduction in double layer capacitance which the model is incapable of predicting since we gave it the parameters extracted from the measurement in 1x PBS.

Although it might be possible to explicitly implement the compensation of the double layer capacitance change with electrolyte concentration in the model from the theory, we do not think that would be very worthwhile for two reasons. First, the relative error for 0.1x PBS is still not that large (compared to Voigt RC implementation for example) and

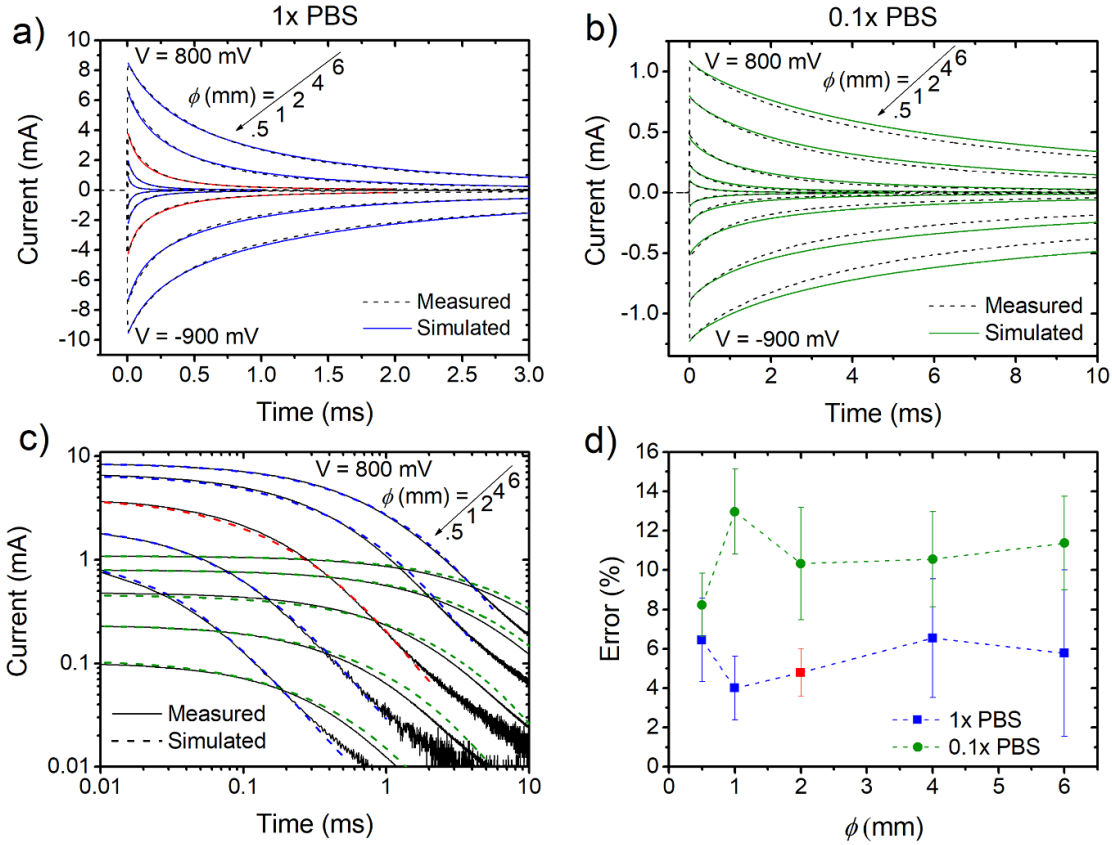

Figure 8. Comparison between simulated and measured currents with a TiN electrode as a response to a short voltage pulse for different electrode diameter and electrolyte concentration combinations. (a) Measured and simulated currents for different electrode diameters in 1x PBS and voltages 0.8 V (positive) and −0.9 V (negative) vs Ag/AgCl reference. Parameters are extracted from the 2 mm electrode (shown in red) and applied to all the other combinations. (b) Same as in (a) but for a 0.1× PBS. (c) Positive current traces from figures (a) and (b) combined in a Log–Log plot to provide improved visibility with largely differing current and time scales. (d) Average error as defined in 5.3 for different diameter-electrolyte combinations. Error for each combination is averaged for 17 voltage pulse amplitudes from −900 to 800 mV in steps of 100 mV vs Ag/AgCl. The error bar represents standard deviation for the 17 voltage amplitudes for each combination.

the model can still be considered usable for electrolyte concentrations variations not larger than 10x which corresponds to a significant conductivity range in which many typical electrical stimulation experiments would fall into. Second, it would be much simpler to just use the electrolyte preparation for electrode characterization that is as similar as possible to the one used in the *in vitro* or *in vivo* experiments.

3.4.2. Variation in stimulus shape

Up to now, we have only used voltage-controlled pulses because it is relatively simple to determine the safe voltage range from the CV that will not cause excessive Faradaicity that can for example cause significant formation of bubbles on the electrode which would make modelling very difficult or outright damage the electrode. In practice though, researchers are often interested in the deposited charge which is much simpler to control with the current controlled pulses.

Thus, we tested the ability of our model to replicate the electrode behaviour for current controlled pulses on biphasic charge balanced cathodic leading pules as a representative waveform. We chose a range of current amplitudes and adjusted the pulse duration such that the maximum voltage on the electrode does not exceed −900 mV vs. Ag/AgCl reference which was the maximum value for all voltage-controlled experiments. The same model parameters as in the previous subsection are used without any further optimization. Simulated and measured voltages are shown in figure 9.

Overall, we observe that the measured and simulated voltages are in agreement in both the cathodic and the anodic part of the pulse and the agreement holds for a range of current amplitudes and pulse durations. The error metric as defined in 5.3 with current replaced by voltage gives us an average error of (7 ± 2) % which is comparable to the error for voltage pules (figures 7 and 8). We can therefore conclude that the model holds similarly well for current controlled stimulation.

3.5. Interpretation of model parameters and model applicability

For bioelectronics applications, be it for electrical stimulation or electrical measurements, electrode impedance is of essential value. As a rule of thumb,

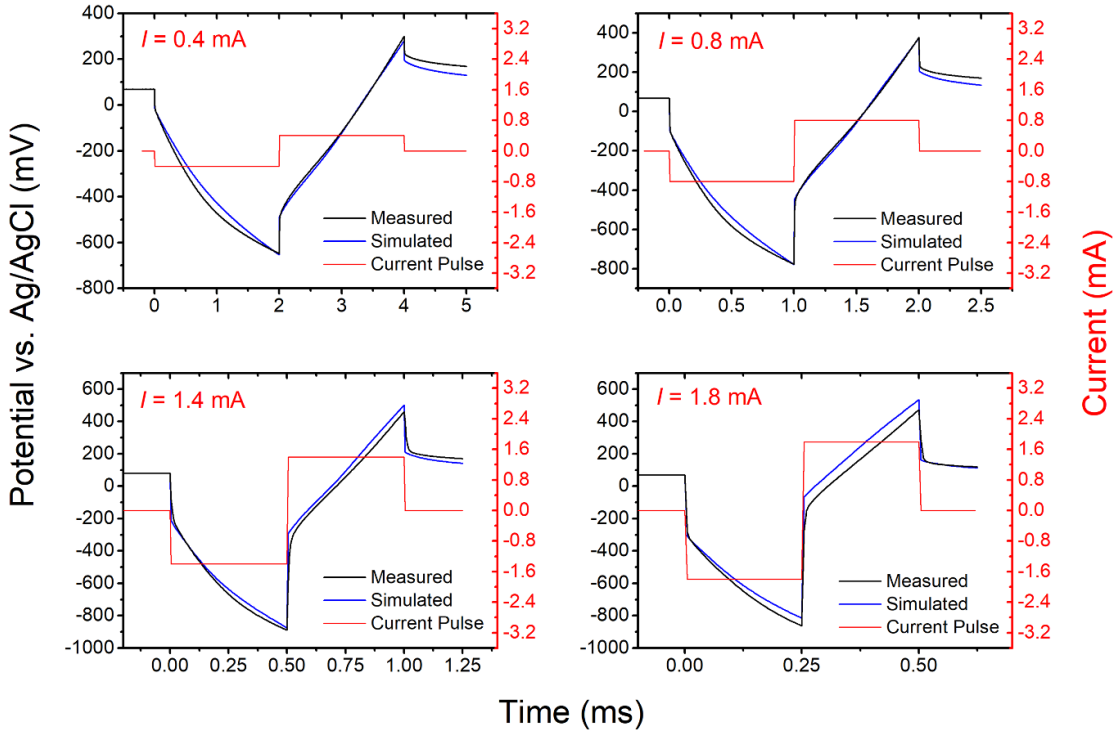

Figure 9. Simulated and measured voltages for a 2 mm diameter TiN electrode in current controlled pulses for different current amplitudes and pulse durations.

low impedance is desirable in most cases, as is high interfacial capacitance and low Faradaic current component. IrOx and TiN emerge as good electrode candidates in this respect. However, subtle effects of electrode geometry and cell-electrode cleft distance may have a profound effect on the stimulation thresholds, as well as on measured signal amplitudes. This work presents a tool to be used in comprehensive numerical models, which would include both the presented realistic electrode model, and a model of a biological system, be it a single cell, a neural bundle or a portion of the central nervous system. In addition, we give an important caveat about using the Voigt RC equivalent circuit to represent most of the presented materials—even though the time-domain implementation of an equivalent RC circuit is simple, the absolute error in modelled delivered charge can easily reach up to 50% for certain materials. If the modelling outcomes differ significantly with the variation of delivered charge of this scale, a more complex model including the distributed CPEs might be necessary. The model has shown to be robust for current-driven stimulation, as well as when used in up to 10x diluted electrolytes. The RC and CPE parameters we give for different materials should be used only as first approximations for the electrode used, and always the fresh model should be built for every new application and every new material.

4. Conclusions

We outlined a method that can be used to estimate and simulate electrode response at the electrode/electrolyte interface for pulsed operation from electrode parameters that can be easily obtained by the common experimental techniques of EIS and FA .This method gives a sub-10% error between measured and simulated currents for a range of materials (Ti,TiN,ITO,Au,Pt,IrOx) and pulsed voltages when the CPE model is used. When using the ideal capacitor instead, the agreement is good only for materials that have a CPE exponent α greater than 0.9. On the other hand, using the CPE has many disadvantages for example, less intuitive physical interpretation of the electrode parameters, complicated implementation in time-dependent simulations, and it is computationally much more demanding than simple Voigt RC electrode representation. It is thus helpful to understand and estimate a possible error that one would make in choosing an RC representation for a particular electrode material and weigh the pros and cons of choosing to use the RC or CPE model.

Data availability statement

The data that support the findings of this study are openly available at the following URL/DOI: https://urn.nsk.hr/urn:nbn:hr:217:393738.

Author contributions

Aleksandar Opančar: investigation (lead); software (lead); methodology (equal); formal analysis (lead); visualization (lead); writing—original draft (supporting); writing—review and editing (equal). **Eric Daniel Głowacki**: conceptualization (supporting); writing—review and editing (equal); funding acquisition (supporting); resources (supporting);**Vedran Đerek**: conceptualization (lead); supervision (lead); writing—original draft (lead); writing—review and editing (equal); methodology (equal); data curation; funding acquisition (lead); project administration.

Conflict of interest

The authors have no conflicts to disclose.

Funding statement

This work has been supported by the Croatian Science Foundation under the Project UIP-2019-04-1753. V Đ and A O acknowledge the support of project CeNIKS co-financed by the Croatian Government and the European Union through the European Regional Development Fund—Competitiveness and Cohesion Operational Programme (Grant No. KK.01.1.1.02.0013), and the QuantiXLie Center of Excellence, a project co-financed by the Croatian Government and European Union through the European Regional Development Fund—the Competitiveness and Cohesion Operational Programme (Grant KK.01.1.1.01.0004). This work was supported by the European Research Council (ERC) under the European Union's Horizon 2020 research and innovation program (E.D.G. Grant Agreement No. 949191), by the Grant Agency of the Czech Republic under Contract No. 23-07432S, and by funding from the National Center for Neurological Research, supported by the Czech Ministry of Education, Youth, and Sports (MEYS CR, LX22NPO5107). Sample fabrication was enabled by CzechNanoLab Research Infrastructure supported by MEYS CR (LM2023051).

Ethics statement

Ethics approval not required.

ORCID iDs

Aleksandar Opančar https://orcid.org/0000-0003-3471-1110
Eric Daniel Głowacki https://orcid.org/0000-0002-0280-8017
Vedran Đerek https://orcid.org/0000-0001-9507-6865

References

[1] Maynard E M, Nordhausen C T and Normann R A 1997 The utah intracortical electrode array: a recording structure for potential brain-computer interfaces *Electroencephalogr. Clin. Neurophysiol.* **102** 228–39
[2] Zeck G and Fromherz P 2001 Noninvasive neuroelectronic interfacing with synaptically connected snail neurons immobilized on a semiconductor chip *Proc. Natl Acad. Sci.* **98** 10457–62
[3] Fromherz P 2002 Electrical interfacing of nerve cells and semiconductor chips *ChemPhysChem* **3** 276–84
[4] Dinyari R, Loudin J D, Huie P, Palanker D and Peumans P 2009 A curvable silicon retinal implant *Technical Digest Int. Electron Devices Meeting, IEDM* (*Baltimore, MD, USA, 7–9 December 2009*) (https://doi.org/10.1109/IEDM.2009.5424291)
[5] Schmidt T *et al* 2022 Light stimulation of neurons on organic photocapacitors induces action potentials with millisecond precision *Adv. Mater. Technol.* **7** 2101159
[6] Silverå Ejneby M *et al* 2021 Chronic electrical stimulation of peripheral nerves via deep-red light transduced by an implanted organic photocapacitor *Nat. Biomed. Eng.* **6** 741–53
[7] Silverå Ejneby M, Migliaccio L, Gicevičius M, Đerek V, Jakešová M, Elinder F and Głowacki E D 2020 Extracellular photovoltage clamp using conducting polymer-modified organic photocapacitors *Adv. Mater. Technol.* **5** 1900860
[8] E K 2014 *Implantable Bioelectronics* ed E Katz (Wiley)
[9] Deshmukh A *et al* 2020 Fully implantable neural recording and stimulation interfaces: peripheral nerve interface applications *J. Neurosci. Methods* **333** 108562
[10] Won S M, Cai L, Gutruf P and Rogers J A 2023 Wireless and battery-free technologies for neuroengineering *Nat. Biomed. Eng.* **7** 405–23
[11] Cai L and Gutruf P 2021 Soft, wireless and subdermally implantable recording and neuromodulation tools *J. Neural Eng.* **18** 41001
[12] Lanmüller H, Sauermann S, Unger E, Schnetz G, Mayr W, Bijak M, Rafolt D and Girsch W 1999 Battery-powered implantable nerve stimulator for chronic activation of two skeletal muscles using multichannel techniques *Artif. Organs* **23** 399–402
[13] Cogan S F, Ludwig K A, Welle C G and Takmakov P 2016 Tissue damage thresholds during therapeutic electrical stimulation *J. Neural Eng.* **13** 021001
[14] Shannon R V 1992 A model of safe levels for electrical stimulation *IEEE Trans. Biomed. Eng.* **39** 424–6
[15] Reilly J P 1998 *Applied Bioelectricity* (Springer)
[16] Merrill D R, Bikson M and Jefferys J G R 2005 Electrical stimulation of excitable tissue: design of efficacious and safe protocols *J. Neurosci. Methods* **141** 171–98
[17] Merrill D R 2010 The electrochemistry of charge injection at the electrode/tissue interface *Implantable Neural Prostheses 2* ed D Zhou and E Greenbaum (Springer) pp 85–138
[18] Ehlich J, Migliaccio L, Sahalianov I, Nikić M, Brodský J, Gablech I, Vu X T, Ingebrandt S and Głowacki E D 2022 Direct measurement of oxygen reduction reactions at neurostimulation electrodes *J. Neural Eng.* **19** 036045
[19] Günter C, Delbeke J and Ortiz-Catalan M 2019 Safety of long-term electrical peripheral nerve stimulation: review of the state of the art *J. Neuroeng. Rehabil.* **16** 13
[20] Harris A R 2020 Current perspectives on the safe electrical stimulation of peripheral nerves with platinum electrodes *Bioelectron. Med.* **3** 37–49
[21] Díaz L *et al* 2020 Ethical considerations in animal research: the principle of 3r's *Rev. Invest. Clin.* **73** 199–209
[22] Singh M, Fuenmayor E, Hinchy E P, Qiao Y, Murray N and Devine D 2021 Digital twin: origin to future *Appl. Syst. Innov.* **4** 36

[23] Wright L and Davidson S 2020 How to tell the difference between a model and a digital twin *Adv. Model. Simul. Eng. Sci.* **7**
[24] Zimmermann J, Budde K, Arbeiter N, Molina F, Storch A, Uhrmacher A M and van Rienen U 2021 Using a digital twin of an electrical stimulation device to monitor and control the electrical stimulation of cells in vitro *Front. Bioeng. Biotechnol.* **9** 765516
[25] Ghazavi A, Westwick D, Xu F, Wijdenes P, Syed N and Dalton C 2015 Effect of planar microelectrode geometry on neuron stimulation: finite element modeling and experimental validation of the efficient electrode shape *J. Neurosci. Methods* **248** 51–58
[26] Buitenweg J R, Rutten W L C and Marani E 2000 Finite element modeling of the neuro-electrode interface *IEEE Eng. Med. Biol. Mag* **19** 46–52
[27] Zimmermann J, Sahm F, Arbeiter N, Bathel H, Song Z, Bader R, Jonitz-Heincke A and van Rienen U 2023 Experimental and numerical methods to ensure comprehensible and replicable alternating current electrical stimulation experiments *Bioelectrochemistry* **151** 108395
[28] Lasia A 2014 *Electrochemical Impedance Spectroscopy and Its Applications* (Springer)
[29] Lukács Z and Kristóf T 2020 A generalized model of the equivalent circuits in the electrochemical impedance spectroscopy *Electrochim. Acta* **363** 137199
[30] Brug G J, van den Eeden A L G G, Sluyters-Rehbach M and Sluyters J H 1984 The analysis of electrode impedances complicated by the presence of a constant phase element *J. Electroanal. Chem.* **176** 275–95
[31] Rossmacdonald J 1984 Note on the parameterization of the constant-phase admittance element *Solid State Ion.* **13** 147–9
[32] Zoltowski P 1998 On the electrical capacitance of interfaces exhibiting constant phase element behaviour *J. Electroanal. Chem.* **443** 149–54
[33] Córdoba-Torres P, Mesquita T J and Nogueira R P 2013 Influence of geometry-induced current and potential distributions on the characterization of constant-phase element behavior *Electrochim. Acta* **87** 676–85
[34] Jorcin J B, Orazem M E, Pébère N and Tribollet B 2006 CPE analysis by local electrochemical impedance spectroscopy *Electrochim. Acta* **51** 1473–9
[35] Huang V M, Vivier V, Orazem M E, Pebère N and Tribollet B 2007 The apparent constant-phase-element behavior of an ideally polarized blocking electrode *J. Electrochem. Soc.* **154** C81
[36] Huang V, Vivier V, Orazem M E, Pebere N and Tribollet B 2007 The apparent cpe behavior of a disk electrode with faradaic reactions: a global and local impedance analysis *ECS Trans.* **3** 567–85
[37] Gablech I, Migliaccio L, Brodský J, Havlíček M, Podešva P, Hrdý R, Ehlich J, Gryszel M and Głowacki E D 2023 High-conductivity stoichiometric titanium nitride for bioelectronics *Adv. Electron. Mater.* **9** 2200980
[38] van Ooyen A, Topalov G, Ganske G, Mokwa W and Schnakenberg U 2009 Iridium oxide deposited by pulsed dc-sputtering for stimulation electrodes *J. Micromech. Microeng.* **19** 074009
[39] de Pauli M, Gomes A M C, Cavalcante R L, Serpa R B, Reis C P S, Reis F T and Sartorelli M L 2019 Capacitance spectra extracted from EIS by a model-free generalized phase element analysis *Electrochim. Acta* **320** 134366
[40] Cantrell D R, Inayat S, Taflove A, Ruoff R S and Troy J B 2008 Incorporation of the electrode–electrolyte interface into finite-element models of metal microelectrodes *J. Neural Eng.* **5** 54–67
[41] Westerlund S 1991 Dead matter has memory *Phys. Scr.* **43** 174–9
[42] Newman J 1970 Frequency dispersion in capacity measurements at a disk electrode *J. Electrochem. Soc.* **117** 198
[43] Opančar A, Đerek V and Glowacki E 2024 Choosing the Right Electrode Representation for Modeling Real Bioelectronic Interfaces: A Comprehensive Guide [Data set] *Prirodoslovno-matematiˇcki fakultet* urn:nbn:hr:217:393738
[44] Bard A J, Faulkner L R and White H S 2022 *Electrochemical Methods: Fundamentals and Applications* (Wiley)